Journal of Fluids and Structures (2002) **16**(3), 295–316
doi:10.1006/jfls.2001.0427, available online at http://www.idealibrary.com on IDEAL®

VORTEX BREAKDOWN FROM A PITCHING DELTA WING INCIDENT UPON A PLATE: FLOW STRUCTURE AS THE ORIGIN OF BUFFET LOADING

M. Özgören

Department of Mechanical Engineering and Mechanics, Lehigh University, Bethlehem PA 18015, U.S.A.

B. Sahin

Department of Mechanical Engineering, Cukurova University, Balcali 01330 Adana, Turkey

AND

D. Rockwell

Department of Mechanical Engineering and Mechanics, Lehigh University, Bethlehem PA 18015, U.S.A.

(Received 23 October 2000 and in final form 28 September 2001)

A delta wing is subjected to both static and dynamic variations of angle-of-attack; the vortices from the wing impinge upon a stationary plate. A technique of high-image-density particle image velocimetry is employed to compare the patterns of vortex development with and without the impingement plate. For the limiting case of static variations of angle-of-attack, the presence of the plate exerts a large influence on the onset of vortex breakdown. In contrast, dynamic (unsteady) variation of angle-of-attack yields changes of breakdown location that are generally similar for cases with and without the impingement plate. The detailed structure of the vortex breakdown-plate interaction is represented by patterns of instantaneous velocity and vorticity, which serve as the origin of buffet-induced loading of the surface of the plate.

1. INTRODUCTION

1.1. Buffeting of Tails and Plates: Surface Loading

Buffeting of aerodynamic surfaces, especially vortex breakdown incident upon the tail of an aircraft, as well as a simulated tail in the form of a plate, have received considerable attention during the last decade. A comprehensive review is provided by Lee (2000). Wolfe *et al.* (1995*a*) assessed a variety of experiments extending over a wide range of Reynolds and Mach number, and correlated the predominant frequency of buffeting. Investigations that involved the measurement of pressure spectra on either a tail or a plate include those of Bean & Wood (1993), Washburn *et al.* (1993), Canbazoglu *et al.* (1995*a*) and Wolfe *et al.* (1995b). Substantial effort has been devoted to characterization of the surface pressure loading and acceleration response and tails of F-series aircraft. Triplett (1983) determined the fluctuations on the tail of a Model F-15 aircraft. Wentz (1987), Ferman *et al.* (1990),

0889–9746/02/030295 + 22 $35.00/0

Zimmerman *et al.* (1989), Shah (1991), Lee & Tang (1992), Martin & Thompson (1991) and Lee *et al.* (1993) characterized the surface pressure spectra on tails of model F/A-18 aircraft. Moses & Huttsell (2000) performed similar types of measurements on the fin of a model F-22 aircraft. Luber *et al.* (1996) assessed the impact of dynamic loads on the design of aircraft. Finally, the buffet response of a fin can be effectively alleviated by active control of its surface, as shown by Ashley *et al.* (1994).

The focus of the foregoing investigations has been, for the most part, on the measurement of localized surface loading, with the intent of calculating the dynamic response of the surface. Links between the physics of the nonstationary flow patterns and the surface loading have not been pursued.

1.2. Control of Buffet Flow Field and Buffet Loading

Although implementation of various types of control techniques for altering the performance of aircraft has been extensively pursued, relatively few investigations have explicitly addressed the consequence of flow control on buffeting of a tail. Bean & Wood (1993) employed tangential blowing at a leading-edge and observed the buffet loading of a tail. Huttsell *et al.* (1997) employed tangential blowing techniques on actual aircraft configurations to control tail buffeting. Sheta *et al.* (2000) undertook a numerical simulation of various tangential blowing techniques as a means to attenuate the buffet of a twin-tail configuration. Özgören *et al.* (2000) employed small-amplitude perturbations of a delta wing, with the intent of simulating control at the leading-edges of a stationary wing, and characterized the buffet flow field along the leading-edge of a plate. Whereas all of the previous investigations aim to control buffeting by manipulating the vortex at, or close to, its origin, Sahin *et al.* (2000) and Gursul & Xie (2000) employed, respectively, small-amplitude perturbations of the leading-edge of the plate and larger amplitude perturbations of an actual tail. Due to an apparent upstream influence, the incident vortex and its interaction with the aerodynamic surface were altered accordingly.

Generally speaking, the effect of large-amplitude, low-frequency motion of a wing on the buffet loading of a downstream aerodynamic surface has not been pursued. Complex maneuvers of an actual aircraft typically occur at relatively low dimensionless frequencies, in comparison with dimensionless frequencies of either vortex breakdown or a shear layer instability from the leading-edge of the wing. Knowledge of the flow distortion along the aerodynamic surface due to these interactions would be insightful.

1.3. Physics of Interaction of Vortex Breakdown with a Tail, Fin or Plate

An understanding of the buffet loading of an aerodynamic surface requires insight into the unsteady flow field of the region of vortex breakdown as it encounters a tail (fin) or plate. Breitsamter & Laschka (1994*a*, *b*, 1998) employed hot-wire anemometry to characterize in detail the fluctuating flow field of the region of vortex breakdown in the absence of a tail. Beutner *et al.* (1995) used a technique of planar Doppler velocimetry to determine the root-mean-square (r.m.s) patterns of the flow field due to vortex–fin interaction. In a series of investigations employing high-image-density particle image velocimetry (PIV), Mayori & Rockwell (1994) and Wolfe *et al.* (1995*b*) characterized the distortion of vortex breakdown upon encounter with a thin flat plate, and Canbazoglu *et al.* (1995*a*, *b*) used a similar approach to characterize the instantaneous patterns of the distortion due to interaction with a tail.

Further insight into the physics of vortex- and vortex breakdown–tail (fin) interaction is provided by the numerical investigations of Rizk & Gee (1992), Gee *et al.* (1995), Kandil

et al. (1995), Rizetta (1996), Kandil & Sheta (1998) and Gordnier & Visbal (1997). Gordnier and Visbal (1997) demonstrate the mechanism of partitioning of the incident vortex due to its direct encounter with the leading-edge of a plate.

Insight into the relationship between the nonstationary flow patterns along an aerodynamic surface, e.g., the tail of an aircraft, and the buffet loading of the surface is provided by the measurements and model of Breitsamter & Laschka (1994*a*, *b*, 1998). They relate the local loading of the surface to the fluctuating angle-of-attack associated with the turbulence at a given location above the surface. The local angle-of-attack varies with time according to the ratio of the local vertical to horizontal velocity. The central link is an analogy to the Kuessner (1954) integral, which relates the loading on a body to fluctuations of angle-of-attack. An important assumption is that flow separation does not occur along the surface. Generally speaking, knowledge of the fluctuating velocity immediately above the surface can yield a basis for understanding the loading of the surface.

1.4. Upstream Influence on Vortex Breakdown Due to a Body or Surface Located within the Vortex

A body or an aerodynamic surface located within the path of a vortex can potentially alter the onset of vortex breakdown, relative to the case of the free vortex. As a consequence, the state of the vortex breakdown incident upon a tail or fin may be altered relative to that based strictly on consideration of a freely evolving vortex in the absence of a body or surface. Reynolds & Abtahi (1987) and Gursul & Yang (1994) showed that a probe and a moderate-sized cylinder could advance the onset of vortex breakdown. Akilli *et al.* (2001) demonstrated that a wire of diameter approximately two orders of magnitude smaller than the vortex diameter can substantially influence the onset of vortex breakdown. These observations, which involve stationary bodies inserted into the vortex, are complemented by those that employ unsteady motion of a tail (Gursul & Xie 2000) and perturbations of the leading-edge of the plate (Sahin *et al.* 2000) to control the location of vortex breakdown.

An important issue is the offset of the center-line of an incident, broken-down vortex; it may modify the vortex at locations upstream of the leading-edge of a plate or tail. That is, the degree of upstream influence, and thereby alteration of the incident vortex, is expected to be largest when the vortex centerline and the leading-edge are aligned, and diminished when they are offset. The physics of this phenomenon should be quantitatively assessed.

1.5. Phase Lag of Vortex Breakdown due to Large-Amplitude Motion of a Wing, Flap or Extension

A delta wing that undergoes relatively large-amplitude variations of, for example, angle-of-attack, gives rise to unsteady development of the vortex. The influence of a body or aerodynamic surface in the path of a vortex may alter this unsteady development; very little is known of this influence. In the absence of such an obstruction, it is well known that the onset of vortex breakdown lags the motion of the wing (Rockwell 1993). Gursul (2000) has reviewed this phase lag concept and provided a model for its occurrence. Relevant investigations involving the motion of a delta wing in the absence of a downstream obstruction include those of Lowson (1964), Woffelt (1987), Atta & Rockwell (1987, 1990), Reynolds & Abtahi (1987), LeMay *et al.* (1990), Magness et al. (1993), Thompson *et al.* (1991), Miau *et al.* (1992), Greenwell & Wood (1994), Gursul & Yang (1995) and Myose *et al.* (1997). Analogous phase lags occur when a flap or wing extension undergoes unsteady motion, as investigated by Deng & Gursul (1997) and Yang & Gursul (1997).

This concept of phase lag is important for buffet loading of aerodynamic surfaces. The streamwise and transverse locations of vortex breakdown, as it impinges upon a plate or tail, are expected to lag the motion of the wing or aerodynamic surface, e.g., LEX, from which it is generated. The nature of this type of phase lag has not been investigated.

1.6. Unresolved Issues and Objectives

The following issues remain unclarified. First of all, a direct comparison of the physics of vortex breakdown with and without a tail (or plate) has not yet been undertaken. More explicitly, the manner in which the location and structure of vortex breakdown are modified in the presence of an aerodynamic surface for the case of a static wing and a static tail (or plate) has remained unexplored. Second, in the event that the wing undergoes pitching motion, the manner in which the presence of a stationary tail or plate located downstream of the wing influences the phase lag of vortex breakdown, relative to the case of no tail (or plate), has remained uninvestigated. Third, the pitching motion of a wing will produce corresponding cross-stream excursions of the location of vortex breakdown relative to a stationary tail (or plate) located downstream of the wing. The modification of the vortex breakdown-plate encounter has not been addressed. One expects large changes in the velocity field that induces buffet loading. These changes will occur in relation to distortion of patterns of vorticity, and this interrelationship requires clarification.

The aim of the present investigation is to employ a technique of high-image-density particle image velocimetry in two planes, one aligned with the axis of the vortex and the other aligned with the cross-flow plane, in order to determine the underlying physics of the issues defined in the foregoing.

2. EXPERIMENTAL SYSTEM AND TECHNIQUES

Experiments were undertaken in a water channel test section having a height of 610 mm and a width of 927 mm. The depth of the water was maintained constant at a value of 559 mm. An overview of the delta wing–plate configuration is illustrated in Figure 1. It is similar to the arrangement used by Sahin *et al.* (2000), for the case where the wing was maintained stationary, and the impingement plate was subjected to small-amplitude controlled oscillations, and by Özgören *et al.* (2000), for which the wing was perturbed at small amplitude and high frequency and the impingement plate was maintained stationary. The essential characteristics of this system are as follows. The delta wing has a chord $C = 222$ mm, a thickness of 3·2 mm and a sweep angle $\Lambda = 75^\circ$. The wing was beveled on the windward side at an angle of 34°. Regarding the impingement plate, it had a chordwise length of $L_p = 162$ mm and a thickness $t_p = 6{\cdot}3$ mm; the leading-edge was beveled at an angle of 5°, and the trailing-edge at 12°. The plate was oriented horizontally in order to examine the effect of the vertical offset of the center-line of the vortex, relative to the leading-edge of the plate, during pitching motion of the wing. During a complex maneuver of an aircraft, such variations of offset are expected to occur. Furthermore, a long plate was employed in order to preclude possible coupling between the leading- and trailing-edge regions. During the entire set of experiments, the distance between the trailing-edge of the delta wing and the leading-edge of the plate was kept at $L = 73$ mm. This distance allowed vortex breakdown to occur upstream of the leading-edge of the plate, over a range of angle-of-attack α of the wing.

Previous investigations have focused on small perturbations of the wing or plate, with the aim of altering the vortex structure at and near the inherent instability frequency of vortex breakdown. In contrast, the focus of the present experiment is on relatively low-frequency, large amplitude pitching motion of the wing, with the goal of determining the overall

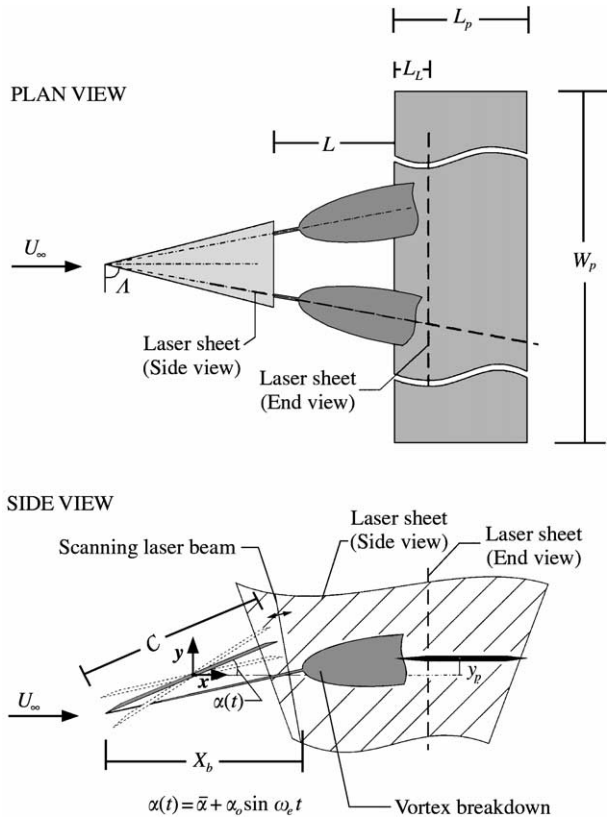

Figure 1. Schematics of delta wing subjected to large-amplitude, low-frequency pitching motion about its midchord, which leads to alteration of the structure of the leading-edge vortex, its breakdown, and its impingement upon a stationary plate. Mean and perturbation angles-of-attack are $\bar{\alpha} = 30^\circ$ and $\alpha_o = 10^\circ$, respectively. Reduced frequency is $k = \pi f_e C/U_\infty = 0{\cdot}74$.

hysteresis effects of vortex breakdown in conjunction with the features of the flow-plate interaction associated with buffet loading. The pitching motion of the wing was according to $\alpha(t) = \bar{\alpha} + \alpha_o \sin \omega_e t$, in which $\omega_e = 2\pi f_e$. The frequency of the pitching motion was maintained constant at $f_e = 0{\cdot}044$ Hz. This frequency was more than an order of magnitude lower than the inherent frequency of vortex breakdown, yet was large enough to allow highly repetitive variations of the time-dependent $x_b(t)$ of vortex breakdown. Moreover, the amplitude of the pitching motion was $\alpha_o = 10^\circ$ for all cases. These excitation parameters corresponded to a value of reduced frequency $k = \pi f_e C/U_\infty = 0{\cdot}74$. Several values of mean angle-of-attack $\bar{\alpha} = 20^\circ$, 24° and 30° were used for cases where the wing was subjected to pitching motion. For cases where static variations of angle-of-attack were considered, values of angle-of-attack $\bar{\alpha} = 24$–30° were employed. The value of freestream velocity was $U_\infty = 42$ mm/s, corresponding to a Reynolds number based on chord C of $\mathrm{Re} = 9{\cdot}34 \times 10^4$. It is well known that the onset of vortex breakdown is relatively insensitive to the value of Reynolds number. The interaction of vortex breakdown with the leading-region of the impingement plate, and the large-scale features of the vortex distortion are expected to be governed primarily by inviscid phenomena, though, of course, the development of the surface boundary layer along the plate and details of possible eruption processes may exhibit a sensitivity to Reynolds number.

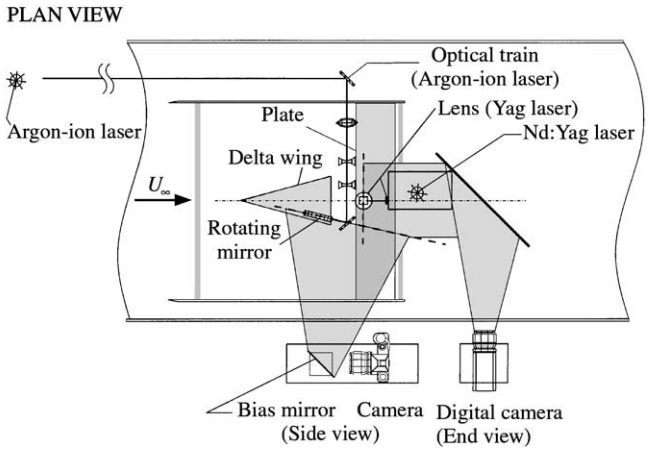

Figure 2. Imaging systems for high-image-density PIV (side view) and DPIV (end view).

Preliminary experiments involved dye injection, in order to determine the location and general structure of vortex breakdown. Moreover, dye was also used to determine the hysteresis of breakdown location as a function of unsteady variations of angle-of-attack. Dye was allowed to seep through a hole on the leeward side of the apex. It marked the center-line of the vortex, and at the onset of breakdown, the width of the dye region increased abruptly. For the case of vortex breakdown from the stationary wing in the absence of the impingement plate, well-known, low-frequency excursions of the vortex breakdown position about an averaged value were observed. In order to account for these excursions, images of the breakdown location were captured at instants corresponding to the maximum value of breakdown location X_b and the minimum value of X_b. Three independent experiments were performed in order to determine three values of minimum and three values of maximum X_b. Then, these values were averaged to obtain the values of X_b shown in the plots herein. The maximum deviation from the average value of X_b was $0{\cdot}076C$ at the minimum value of angle-of-attack $\alpha = 28^\circ$ and decreased to a substantially smaller value of $0{\cdot}028C$ at the maximum angle-of-attack $\alpha = 45^\circ$. On the other hand, the presence of the impingement plate stabilized the location of vortex breakdown, and a maximum deviation of $0{\cdot}03C$ was observed for all values of α. The uncertainty in the detection of the vortex breakdown position was insignificant relative to the aforementioned deviations, which are inherent features of the vortex unsteadiness. Images were recorded on high-resolution film, then digitized at 125 pixels/mm in order to determine the breakdown position. The parallax effect was accounted for by the use of simple trigonometric relations.

High-image-density particle image velocimetry was employed to determine the instantaneous flow patterns. These patterns were characterized over two principal planes, as illustrated in the schematic of Figure 1. One plane was coincident with the center-line of the vortex. The other plane was parallel to the leading-edge of the plate; it provided a representation of the vortex structure in the cross-flow plane. These two locations of the laser sheet are referred to as side and end views, respectively.

Figure 2 shows an overview of the lasers, optical components and camera systems employed for the laser sheets corresponding to the side and end views. For the side view, an Argon-ion laser beam of 1 mm diameter passed through an optical train, and eventually impinged upon a rotating polygonal mirror, which had eight facets. This configuration generated a laser beam scanning at a rate of 75 Hz. This scanning beam generated a laser

sheet, which was coincident with the center-line of the vortex breakdown. The sheet appears as a bold line in the plan view of Figure 2. Seeding of the flow involved metallic-coated particles, which had a nominal diameter of 14 μm. They were illuminated by the scanning laser beam, and their images were recorded using a film-based camera. The camera was operated at a shutter speed of 1/15 s and an f-stop, f = 5. High-resolution film of 300 lines/mm was used. In order to avoid issues associated with directional ambiguity, a bias mirror was located immediately in front of the camera lens. This arrangement provided positive displacements of all particle image patterns recorded on the film. The film was digitized at a resolution of 125 pixels/mm, then interrogated to determine the instantaneous velocity field.

On the other hand, for the end view imaging, which was done independently, a technique of DPIV was employed. The laser illumination source was a double-pulsed Yag laser, and the laser sheet was generated by a cylindrical lens. Images were recorded on a digital camera having a resolution of 1008 × 1018 pixels. The image acquisition was at a rate of 30 frames/s, corresponding to 15 pairs of images per second. A frame-to-frame correlation technique was employed to calculate the velocity field.

For the case of the film-based PIV technique, the area of the interrogation corresponded to 90 pixels × 90 pixels, and approximately 40–60 particle images were located within this area. For the DPIV approach, the interrogation area was 32 pixels × 32 pixels; it contained approximately 15–25 particle images. In accord with the Nyquist criterion, a 50% overlap was employed for successive interrogations.

For the side view (film-based PIV approach), the magnification was $M = 1:4{\cdot}52$, which gave an effective grid size of 1·63 mm × 1·63 mm on the physical plane of the laser sheet. Images of the flow pattern were acquired at a framing rate of 1·55 frames/s. With respect to the end view (DPIV technique), the magnification was $M = 1:7{\cdot}72$, which corresponded to an effective grid size of 2·07 mm × 2·07 mm in the plane of the laser sheet.

The field of view of the acquired images was 151·3 mm × 97·3 mm for the side view and 124·4 × 126·5 mm^2 for the end view. The total number of velocity vectors was approximately 5 734 for the side view and 3 782 for the end view. A Gaussian filter with a factor $p = 1{\cdot}3$ was applied to calculate the velocity field. No additional filtering of the data was carried out.

As described in the investigation of Özgören *et al.* (2000), averaged representations of velocity and vorticity were obtained by averaging images of the flow pattern. In order to obtain averaged images, a total of N images were averaged at a given location (x, y). The average values of velocity and vorticity, as well as the root-mean-square (r.m.s) values of velocity, were obtained according to the following equations:

$$\langle V \rangle = \frac{1}{N}\sum_{n=1}^{N} V_n(x, y), \quad \langle \omega \rangle = \frac{1}{N}\sum_{n=1}^{N} \omega_n(x, y), \tag{1a, b}$$

$$v_{\text{r.m.s.}} = \left\{\frac{1}{N}\sum_{n=1}^{N} [v_n(x, y) - \langle v(x, y)\rangle]^2\right\}^{1/2}, \quad \omega_{\text{r.m.s.}} = \left\{\frac{1}{N}\sum_{n=1}^{N} [\omega_n(x, y) - \langle \omega(x, y)\rangle]^2\right\}^{1/2}. \tag{1c, d}$$

3. ONSET AND DEVELOPMENT OF VORTEX BREAKDOWN WITH AND WITHOUT IMPINGEMENT PLATE

3.1. Stationary Wing

Figure 3a shows the onset of vortex breakdown X_b normalized by the wing chord C as a function of static angle-of-attack α. For these experiments, the value of α was adjusted, the

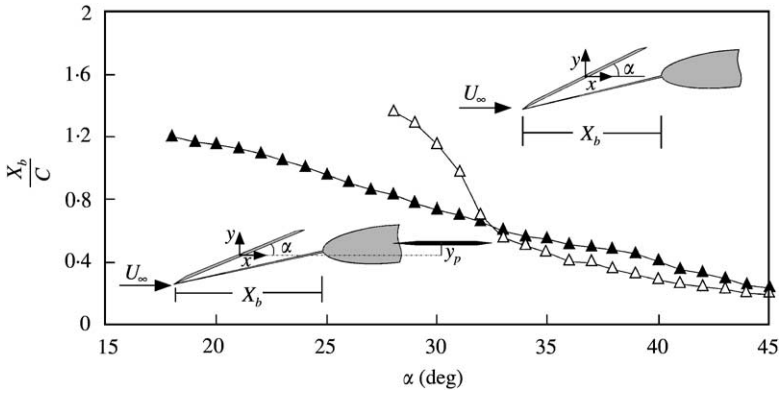

Figure 3(a). Variation of location of vortex breakdown with static angle-of-attack of stationary wing. Breakdown locations are compared: ▲, in the presence of impingement plate; △, in the absence of impingement plate.

flow was allowed to attain equilibrium, and the value of the vortex breakdown position X_b was determined via the dye injection technique described in Section 2. For all experiments, the plate was located at a distance of $y_p/C = 0{\cdot}14$ above the pitching axis of the wing. This location provided direct impingement of the central portion of the vortex breakdown region upon the leading-edge of the plate at an angle-of-attack $\alpha = 24^\circ$. As indicated in Figure 3a, when the plate is present, and the angle-of-attack is lower than approximately $\alpha = 32^\circ$, the vortex breakdown position is advanced in the upstream direction. That is, it occurs at a lower value of X_b/C, relative to the case without the plate. Over this range of α, the offset between the centerline of the vortex and the leading-edge of the plate is minimal, as indicated in the images of averaged vorticity in the left column of Figure 3b. In these images, the onset of vortex breakdown *vb* is defined to occur at the leading-edges of the contours of constant positive and negative vorticity. This definition is in accord with the theoretical basis of Brown & Lopez (1990), whereby the onset of breakdown corresponds to a switch in the sign of azimuthal vorticity. At $\alpha = 24^\circ$, vortex breakdown does not occur within the field of view when the plate is absent. In presence of the plate, it is located near the trailing-edge. At $\alpha = 30^\circ$, breakdown occurs just downstream of the trailing-edge without the plate. With the plate present, it moves out of the field of view to a location well upstream of the trailing-edge.

The upstream advancement of the breakdown position relative to the case of no edge, evident by comparison of the left and right columns of Figure 3b, is in accord with the observations of Reynolds & Abtahi (1987) and Gursul & Yang (1994), who placed a probe and a moderate-sized /cylinder along the center-line of the vortex. Furthermore, Akilli *et al.* (2001) found that a wire two orders of magnitude smaller than the vortex diameter could have a similar effect when oriented orthogonal to, but coincident with, the center-line of the vortex. All of these observations are related to the upstream transmission of disturbances through the vortex, as described in previous theoretical works summarized by Akilli *et al.* (2001). These works include Leibovich (1984), Wang & Rusak (1997) and Rusak *et al.* (1998).

On the other hand, for higher values of $\alpha \gtrsim 32^\circ$ in Figure 3a, the difference between values of X_b/C with and without the plate is relatively small. For $\alpha > 32^\circ$ in Figure 3a, the offset between the vortex centerline and the plate becomes large (cf. $\alpha = 35^\circ$ and 30° in Figure 3c). As a consequence, the upstream transmission of information is not as effectively accomplished. Furthermore, the onset of breakdown moves closer to the apex of the wing at larger α; in this limiting case, breakdown seems to be primarily controlled by the vortex characteristics immediately downstream of the apex.

The averaged images of Figures 3b were obtained from instantaneous images of the type shown in Figure 3c. The left column of images corresponds to cases with the plate and the right column to the cases without the plate. Consider, first of all, the images in the left column. At the lowest angle-of-attack $\alpha = 24^\circ$, the onset of vortex breakdown occurs immediately downstream of the trailing-edge of the wing, and instantaneous positive (thick white line) patterns and negative (thin white line) patterns indicate a staggered arrangement of vorticity concentrations that represent the helical mode of instability. Subsequent interaction with the leading-edge of the plate yields substantial distortion. At $\alpha = 30^\circ$, vortex breakdown occurs at a significant distance upstream of the trailing-edge of the wing and is not evident in the field of view. Large-scale clusters of vorticity concentrations are evident as they interact with the plate. Finally, at $\alpha = 35^\circ$, the onset of breakdown (not visible) occurs even further upstream. Furthermore, the wake-like region of breakdown is shifted upward, such that almost the entire pattern of vorticity is above the plate. For the images in the right column of Figure 3c, corresponding to the case without the impingement plate, vortex breakdown does not occur within the field of view at $\alpha = 24^\circ$. It is located well downstream of the trailing-edge of the wing (compared to the image of Figure 3b). Only low-level, small-scale concentrations of vorticity are evident. At $\alpha = 30^\circ$, breakdown does occur, and it gives rise to a staggered arrangement of vorticity concentrations, which are similar in concept to those at $\alpha = 24^\circ$ with the plate present. At $\alpha = 35^\circ$, the onset of vortex breakdown is a substantial distance upstream of the trailing-edge of the wing. The wake-like structure of the vortex breakdown region is associated with larger-scale concentrations of vorticity.

3.2. Pitching Wing

From the plot of Figure 3a, along with the images shown in Figures 3b and 3c, it is evident that the presence of the impingement plate can substantially alter the onset of vortex breakdown for the case of the stationary wing. An important issue is whether this type of influence extends to vortex breakdown generated from a pitching delta wing.

Figure 4 shows the instantaneous location of vortex breakdown $X_b(t)$ normalized by the wing chord C as a function of the instantaneous angle-of-attack $\alpha(t)$ for cases without and with the impingement plate. In the absence of a plate, it is well known that the onset of vortex breakdown lags the motion of the wing, and the end consequence is the generation of the type of dynamic hysteresis loops of vortex breakdown shown in Figure 4. These loops are shown for three values of mean angle-of-attack $\bar{\alpha} = 20^\circ$, 24° and 30°. At the two lowest values of $\bar{\alpha} = 20^\circ$ and 24°, data were not acquired during a portion of the downstroke. It is remarkable that for all values of $\bar{\alpha}$, the difference between the instantaneous locations of vortex breakdown $X_b(t)/C$ with and without the plate is relatively small. A discernible exception occurs at the highest values of $\alpha(t)$ at the largest mean angle-of-attack $\bar{\alpha} = 30^\circ$. It is therefore evident that the dynamic nature of the vortex breakdown process and thereby the phase lag are not significantly influenced by the presence of the impingement plate, at least in a general sense.

Figures 5a and 5b represent, respectively, cases with and without the impingement plate. They show instantaneous patterns of vorticity corresponding to dynamic variations of angle-of-attack $\alpha(t)$ for a mean angle-of-attack $\bar{\alpha} = 30^\circ$. In each layout, images are shown for three successive instants during the oscillation cycle. Moreover, in each of the images of Figure 5a and 5b, the instantaneous angle-of-attack $\alpha(t)$ is indicated at the upper right corner, as is the dimensionless time $t^* = tU_\infty/C$. Consider, first of all, the top image of Figure 5a, which corresponds to $\alpha = 30^\circ$. The location of vortex breakdown *vb* is within the

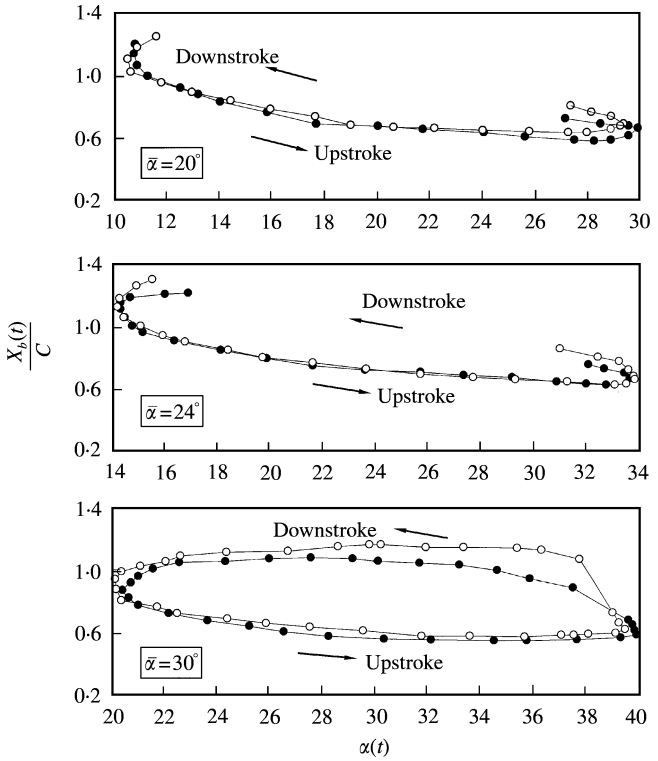

Figure 4. Comparison of dynamic hysteresis loops of vortex breakdown as a function of angle-of-attack: ●, in the presence of the impingement plate; ○, in the absence of the impingement plate. Amplitude of the pitching motion is $\alpha_o = 10^{\circ}$ and the reduced frequency is $k = \pi f_e C/U_\infty = 0{\cdot}74$ for all cases.

field of view and near the trailing-edge. The centerline of the vortex breakdown region, which is defined by patterns of positive and negative azimuthal vorticity, is slightly above the leading-edge of the plate. In the second image, corresponding to $\alpha = 39.5^{\circ}$, the center-line of the vortex breakdown is located above the plate, and in the third image at $\alpha = 23{\cdot}4^{\circ}$, it is approximately aligned with the leading-edge. These images can be compared with those of Figure 5b, which represent cases without the plate. It is evident that the onset of vortex breakdown, when it is detectable, is located slightly further downstream for the case without the impingement plate.

The issue arises as to the insensitivity of the dynamic variations of the vortex breakdown position $X_b(t)$ versus angle-of-attack $\alpha(t)$; that is, these variations of $X_b(t)$ are very similar for cases with and without the impingement plate. During a given pitching cycle, the offset of the vortex center-line with respect to the leading-edge of the plate varies substantially, as shown in Figure 5a for the case of the impingement plate. In essence, this means that the location of vortex breakdown X_b does not have the opportunity to relax to an equilibrium state, unlike the aforementioned case of vortex breakdown from a stationary wing incident upon a plate. That is, the vortex dynamics appears to be controlled primarily by the wing motion, rather than by the upstream influence from the region of the impingement plate.

These observations of the vortex breakdown characteristics for the case of the pitching wing provide a basis for assessment of the corresponding end views of the vortex break-down/plate interaction, which are addressed in the next section.

4. EVOLUTION OF VORTEX–PLATE INTERACTION IN CROSS-FLOW PLANE: PATTERNS OF VORTICITY

Patterns of instantaneous vorticity ω and averaged vorticity $\langle\omega\rangle$, as well as corresponding velocities V and $\langle V\rangle$, are shown in the images of Figures 6 and 7 for the cross-flow planes defined in the schematics of Figures 1 and 2. The streamwise location of the cross-flow laser sheet is designated by the thin, vertical white line in Figure 5a. The angle-of-attack α and the dimensionless time t^* elapsed during the pitching cycle are designated on each set of images.

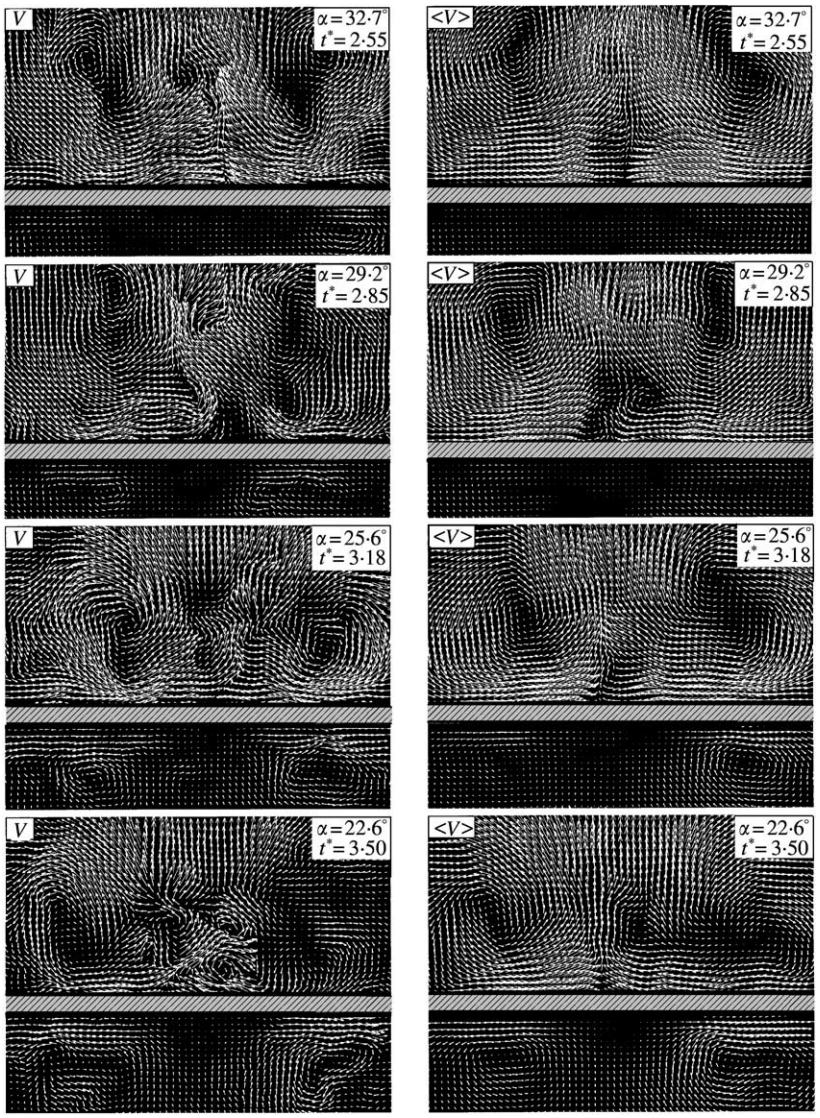

Figure 7(a). Cross-section of vortex breakdown–plate interaction at a location $0{\cdot}185L_p$ downstream of the leading-edge of the plate, corresponding to the thin vertical line in Figure 5a. Delta wing is pitching at reduced frequency $k = \pi f_e C/U_\infty = 0{\cdot}74$. Instantaneous vorticity fields (left column) and averaged vorticity fields (right column) are shown for variations of angle-of-attack α of the wing and dimensionless time $t^* = tU_\infty/C$. Mean angle-of-attack and pitching amplitude of delta wing are $\bar{\alpha} = 30^\circ$ and $\alpha_o = 10^\circ$.

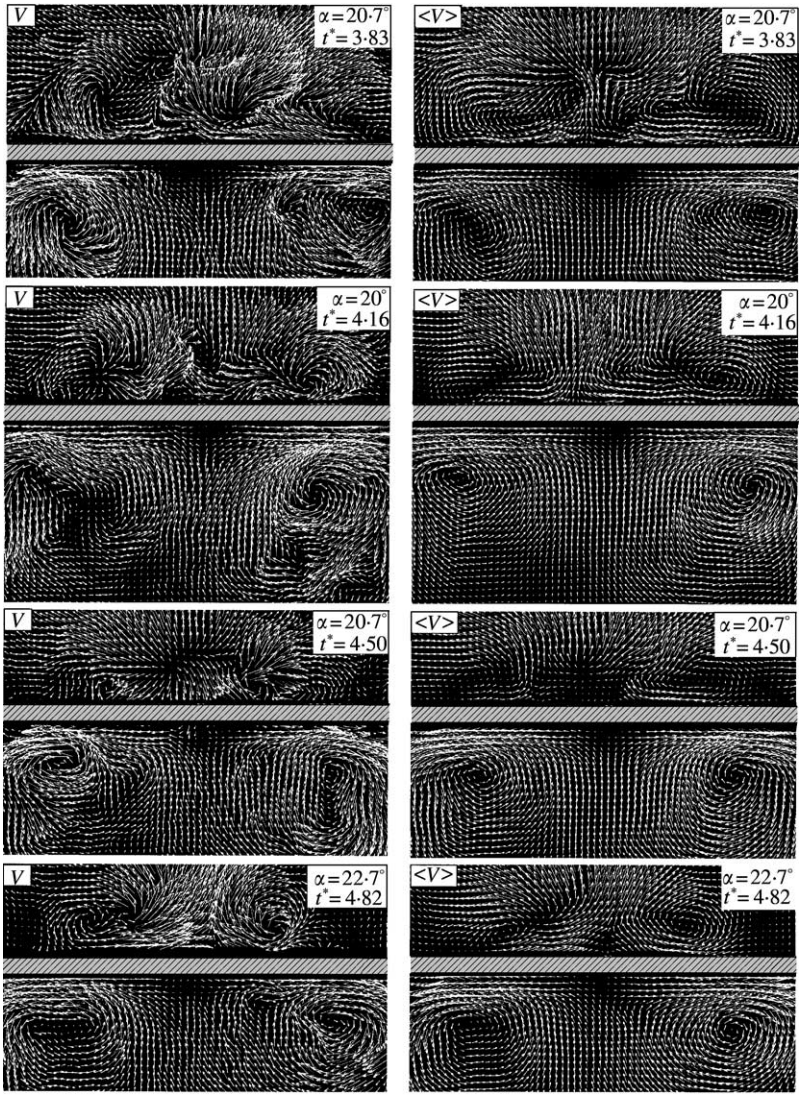

Figure 7(b). Cross-section of vortex breakdown–plate interaction at a location $0{\cdot}185L_p$ downstream of the leading-edge of the plate, corresponding to the thin vertical line in Figure 5a. Delta wing is pitching at reduced frequency $k = \pi f_e C/U_\infty = 0{\cdot}74$. Instantaneous velocity fields (left column) and averaged velocity fields (right column) are shown for variations of angle-of-attack α of the wing and dimensionless time $t^* = tU_\infty/C$. Mean angle-of-attack and pitching amplitude of delta wing are $\bar{\alpha} = 30^\circ$ and $\alpha_o = 10^\circ$.

Furthermore, the location X_b of vortex breakdown for each image set can be determined for each value of α from Figure 4.

Figures 6a and 6b directly compare the contours of constant instantaneous vorticity ω (left column) and averaged vorticity $\langle\omega\rangle$ (right column) for successive values of instantaneous angle-of-attack $\alpha(t)$ and dimensionless time $t^* = tU/C$. Images of averaged vorticity $\langle\omega\rangle$ were obtained by considering a total of four images at each respective phase of the oscillation cycle of the pitching delta wing. These images, which emphasize the large-scale, repetitive vortical structures, are intended to serve as a guide for the interpretation of

instantaneous patterns of ω. Contours of $\langle\omega\rangle$ clearly show the positive (thick white line) and negative (thin white line) projections of streamwise vorticity for the two principal vortices and their distortion upon encounter with the plate. Examination of the images of Figures 6a and 6b reveals a number of phenomena, as described in the following.

4.1. Generation of Concentrations and Layers of Secondary Vorticity Adjacent to Surface of Plate

Considering the images of Figure 6a and 6b, especially the instantaneous representations above the surface of the plate, a concentration of positive vorticity immediately adjacent to the surface of the plate often appears beneath a corresponding concentration of negative vorticity, and conversely. These concentrations appear somewhat randomly in spatial position from one image to the next. In concept, the generation of a vorticity concentration from a solid surface due to a concentration of vorticity of opposite sign above the surface is well documented in a range of investigations, as summarized by Doligalski *et al.* (1994).

On the other hand, in the region below the plate, well-defined layers of distributed vorticity are clearly evident when a significant fraction of the incident vortex system is partitioned below the plate. That is, at angle-of-attack $\alpha = 25.6^\circ$, well-defined layers of vorticity are evident along the lower surface of the plate and, in fact, these layers persist in subsequent images in Figures 6a and 6b. Such layers are clearly evident in images of both ω and $\langle\omega\rangle$.

4.2. Spacing of Major Concentrations of Vorticity Above and Below the Plate

Consider the images of averaged vorticity $\langle\omega\rangle$ in Figures 6a and 6b. As the value of dimensionless time t^* increases, an increasing fraction of the incident vorticity concentrations is partitioned to the region beneath the plate. For all values of $t^* = tU/C$, the distance between these concentrations remains relatively large. On the other hand, the remaining portions that are partitioned to the region above the plate move relatively close together at larger values of t^*. This difference in spacing between vortices on the upper and lower sides of the plates is apparently due to vortex induction. The coexistence of the actual vortices with their corresponding image vortices within the plate results in a tendency for the upper vortex system to move together and the lower system to move apart. This effect was suggested in the limiting situation of a stationary wing and plate in the investigation of Mayori & Rockwell (1994). In addition, the numerical simulation of Gordnier & Visbal (1997), for a stationary wing and plate system, shows a similar difference in spacing between the partitioned vortices on the upper and lower sides of the plate.

4.3. Simultaneous Presence of Small- and Large-Scale Concentration of Vorticity

The instantaneous patterns of vorticity of Figures 6a and 6b, especially those extending from $t^* = 2{\cdot}55$ to $4{\cdot}16$, show small-scale concentrations of vorticity of opposite sense intermingled with the large-scale concentrations. In the averaged images, especially those extending from $t^* = 2{\cdot}55$ to $3{\cdot}18$, it is evident that the small-scale vorticity concentrations of opposite sense exist in the region between the two large-scale, primary vortices. The origin of these small-scale vortical structures may be due to two sources. First of all, prior to encounter with the plate, concentration of vorticity may arise about the periphery of each large-scale vortex from the three dimensionality of the breakdown process. Second, periodic eruption of the surface boundary layer induced by the large-scale vortex adjacent to the

plate can lead to successive, small-scale vorticity concentration, in the manner described by Gordnier & Visbal (1995) and Cipolla & Rockwell (1998).

5. EVOLUTION OF VORTEX–PLATE INTERACTION IN CROSSFLOW PLANE: PATTERNS OF VELOCITY

The images of Figures 7a and 7b show instantaneous V and averaged $\langle V \rangle$ patterns of velocity vectors corresponding to the contours of constant vorticity exhibited in Figures 6a and 6b. The major features of these patterns are described in the following.

5.1. Half-Saddle Distributions of Velocity: Convergence of Patterns of Velocity Vectors at the Plane of Symmetry

Consider the patterns of averaged velocity $\langle V \rangle$ shown in the right columns of Figures 7a and 7b. At the highest angle-of-attack $\alpha = 32{\cdot}7^\circ$, which occurs at $t^* = 2{\cdot}55$, the large-scale vortex system is associated with a pattern of velocity vectors that converges at the vertical plane of symmetry of the plate. According to topological concepts based on critical point theory, this pattern corresponds to a half-saddle point at the locations where the corresponding streamlines would meet at an elevation immediately adjacent to the plate. Away from the surface of the plate, the velocity vectors are directed upwards. This general pattern along the upper surface of the plate persists, with some irregularities, to $\alpha = 20^\circ$, corresponding to $t^* = 4{\cdot}16$. Over the time span from $t^* = 2{\cdot}55$ to $4{\cdot}16$, the saddle point drifts to the left, then to the right at $t^* = 4{\cdot}82$. This observation suggests a low-frequency variation of the saddle point location. At larger values of $\alpha = 20{\cdot}7^\circ$ and $22{\cdot}7^\circ$, a saddle point adjacent to the surface of the plate is not so well defined.

5.2. Stagnation Regions of Patterns of Velocity Vectors: Divergence of Patterns at Plane of Symmetry

As increasing fractions of the incident vortex system are partitioned below the plate, a stagnation region forms along the lower surface of the plate. It is located midway between the centers of the swirl patterns of velocity vectors. This stagnation pattern is first evident at $\alpha = 25{\cdot}6^\circ$ and becomes more sharply defined at subsequent values of α in Figures 7a and 7b. To be sure, the corresponding streamline pattern would also exhibit a half-saddle point analogous to that observed along the upper surface of the plate; on the lower side of the plate, the corresponding streamlines are directed away from, rather than towards the vertical plane of symmetry. In this section, this region is referred to as a stagnation region, since it represents a region of very low velocity magnitude, relative to that occurring on the upper side of the plate.

5.3. Instantaneous Deviations from the Averaged Patterns of Velocity

The concepts of half-saddle point and a stagnation region, which were defined on the basis of the averaged images shown in the right columns of Figures 7a and 7b, are, in some cases, discernible in the corresponding patterns of instantaneous velocity as well. The patterns of instantaneous velocity can exhibit substantially more complex forms, especially for the region above the plate. For example, at $\alpha = 25{\cdot}6^\circ$, the instantaneous pattern of V does not exhibit a single, well-defined half-saddle. Rather, the simultaneous presence of a number of vorticity concentrations along the plate produces several adjacent swirl patterns of velocity vectors. Additional patterns of distortion are shown at the other values of α in the left

columns of Figures 7a and 7b. The buffet model of Breitsamter & Laschke (1994*a*, *b*, 1998) requires the instantaneous vertical component of velocity v, in conjunction with the instantaneous out-of-plane velocity component w at representative spatial locations along the surface of the plate, with the assumption of no significant flow separation from the surface. It is evident that the large variation with time t^* of the instantaneous patterns of Figures 7a and 7b will yield substantial fluctuations of the v component of the buffet velocity. Moreover, the spanwise correlation of the v component fluctuations is not necessarily dictated by a single length scale, e.g., the spanwise distances between the largest scale vortical structures. The patterns of velocity suggest multiple scales of the swirl patterns of velocity vectors.

6. INTERRELATIONSHIP BETWEEN PATTERNS OF VORTICITY AND VELOCITY: CONSEQUENCE FOR BUFFET VELOCITY DISTRIBUTIONS

Taken together, the patterns of velocity and vorticity described in Figures 6 and 7 have important consequences for the vortex-induced loading of the surface of the plate. As shown in the preceding sections, the type of imaging performed in this investigation allows acquisition of a sequence of velocity images, then extraction of the spatial distribution of vertical, or normal, velocity as a function of time. The potential for employing this velocity component as an input to a buffet model is described in Section 1.3. In turn, these patterns of velocity can be directly compared to the corresponding patterns of vorticity, in order to reveal as to how distortion of the vortical structures is related to the patterns of vertical buffet velocity. Our present considerations are twofold. First of all, the aim is to assess the relationship between the instantaneous distributions of vorticity and the corresponding instantaneous patterns of vertical velocity. Second, the sensitivity of the spatial distributions of buffet velocity to distance from the surface of the plate will be addressed.

6.1. Effect of Vortex Partitioning on Patterns of Vorticity in Relation to Patterns of Vertical Buffet Velocity

Figure 8 shows a direct comparison of patterns of instantaneous vorticity ω and vertical velocity v at two critical instants during the vortex–plate interaction. The top row corresponds to the situation where the vortex system is located above the surface of the plate, and the bottom row of images to the scenario where the incident vortices have been split upon encounter with the plate. In the image at the upper left part, large-scale vortical structures are generally discernible and, between them, smaller-scale concentrations of positive and negative vorticity are evident. The corresponding distribution of vertical velocity at the upper right indicates a substantial magnitude of upward (positive) vertical velocity in the region between the two large-scale concentrations of vorticity. Near the left and right boundaries of the image, a region of high downward vertical velocity exists above the surface of the plate. It is evident that the small-scale concentrations of vorticity between the large-scale vortical structures do not produce local changes in the sign of the vertical buffet velocity; rather, its sign everywhere corresponds to the induced velocity between the largest vortical structures.

For the case where the vortex system is split upon its encounter with the plate, as shown in the bottom row of images of Figure 8, a distinctly different pattern of vertical velocity distribution exists. Along the upper surface of the plate, the vertical velocity is positive upward, due primarily to the induced updraft between the two concentrations of vorticity. Only very low-level regions of negative vertical velocity exist on either side of this positive region. This contrasts with the image at the upper right part of Figure 8. It is therefore

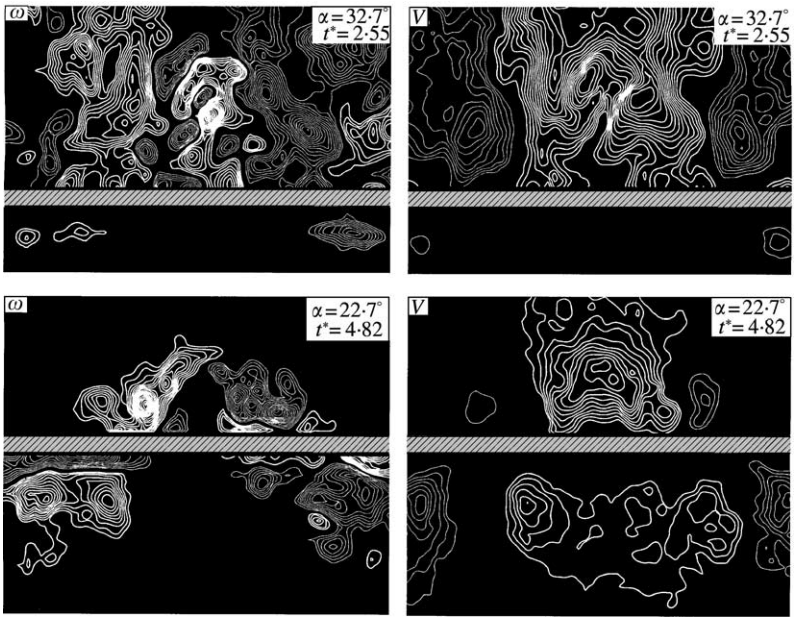

Figure 8. Contours of instantaneous vorticity (left column) and instantaneous vertical velocity (right column). Minimum and incremental values of instantaneous vorticity ω are $\omega_{min} = \pm 1\ s^{-1}$ and $\Delta\omega = 0{\cdot}5\ s^{-1}$, respectively. For vertical velocity v contours, $v_{min} = \pm 5$ (mm/s) and $\Delta v = 2{\cdot}5$ (mm/s), respectively.

evident that partitioning of the incident vortex system, which is represented by the lower set of images, yields a region of large vertical velocity between them, and insignificant vertical velocity exterior to them. Along the lower surface of the plate, a broadly distributed, lower level region of upward (positive) vertical velocity is evident in the central portion of the image and regions of negative vertical velocity exist near the boundary of the image. This type of pattern does not exist along the lower surface of the plate for the case where the vortex system remains above the surface of the plate, as in the top row of images.

6.2. Variation of Distributions of Vertical Buffet Velocity with Distance from Surface of Plate

It is envisioned that a typical model for the buffet loading will require the distribution of buffet velocity along a constant elevation from the surface. The issue then arises as to the sensitivity of the velocity magnitude, as well as its overall distribution, to the displacement from the plate surface. Figure 9a shows the instantaneous distribution of vertical buffet velocity for the case where the vortex system remains above the plate. Four horizontal white lines designate reference heights for evaluation of the velocity distribution. They are indicated as $y = 70$, 75, 80, and 85. In the plots shown at the bottom of Figure 9a, the distributions of the vertical buffet velocity v versus z have a generally similar form, but with significantly different peak magnitudes.

Figure 9b represents the case where the incident vortex system is split by the plate. For both the regions above and below the plate, the general form of the vertical velocity distributions, as a function of distance from the surface of the plate, is again similar, but with differing magnitudes. Above the plate, for example, the peak positive value of buffet velocity

at $y = 85$ substantially exceeds that at $y = 70$. Below the plate, along the line closest to the plate, i.e., $y = 55$, the magnitude of v becomes very small and the general form of the distribution is substantially distorted, relative to the distributions of $y = 50$–40.

Based on these observations of Figures 9a and 9b, it appears that a zonally averaged distribution of buffet velocity might be an appropriate representation of its effective magnitude and distribution. That is, a spatially averaged vertical velocity over a finite horizontal band would alleviate limitations associated with consideration along a single elevation from the surface of the plate.

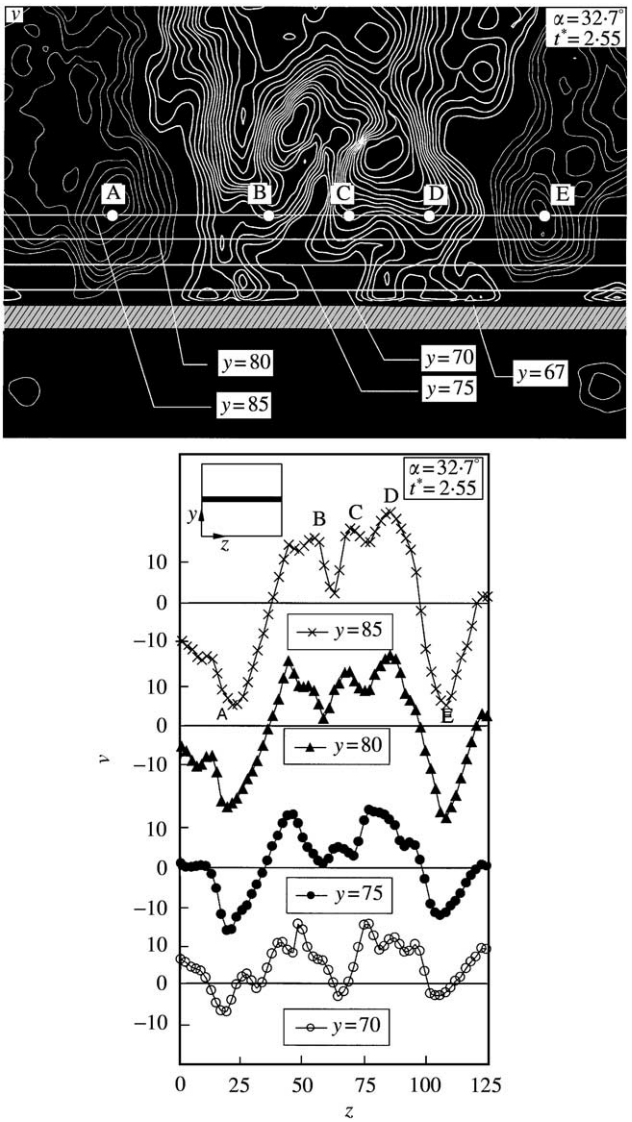

Figure 9(a). Contours of instantaneous vertical velocity v (top image) and distributions of v along horizontal lines indicated in the image. Instantaneous angle-of-attack is $\alpha = 32{\cdot}7^\circ$ and dimensionless time is $t^* = tU_\infty/C = 2{\cdot}55$. Minimum and incremental values of instantaneous vertical velocity contours in image are $v_{\min} = \pm 5$ (mm/s) and $\Delta v = 2{\cdot}5$ (mm/s), respectively. Dimensions of v are mm/s and z is mm.

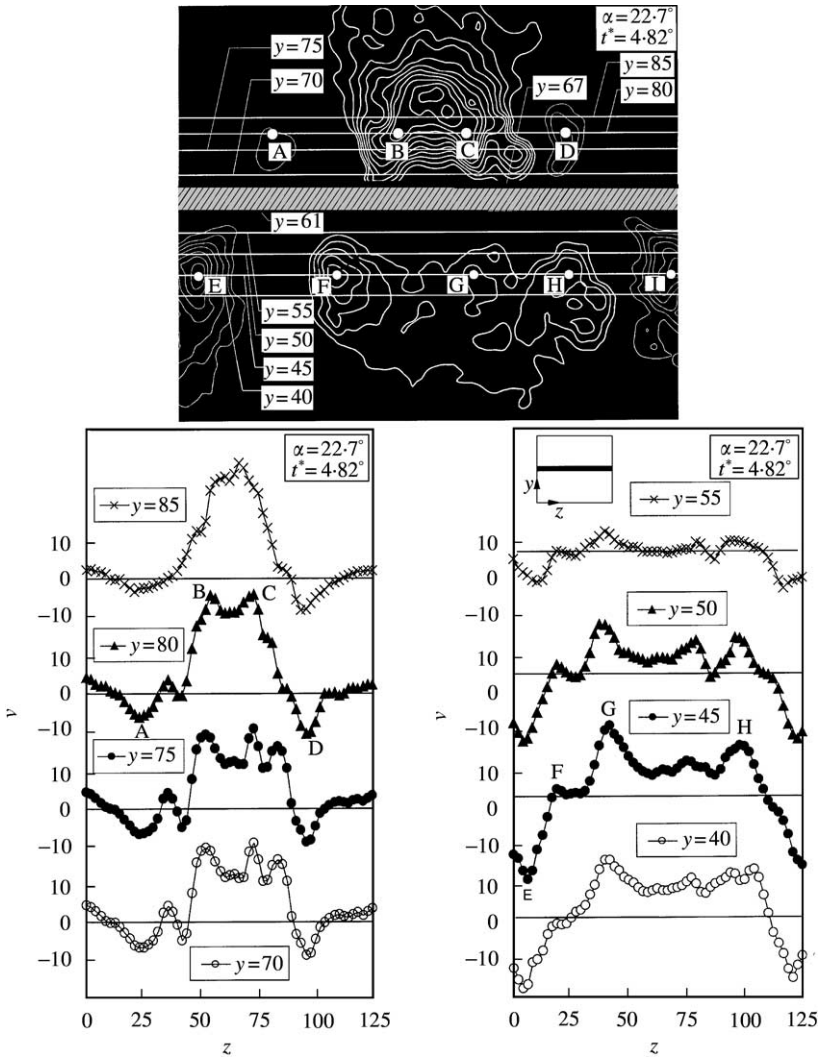

Figure 9(b). Contours of instantaneous vertical velocity v (top image) and distributions of v along horizontal lines indicated in the image. Instantaneous angle-of-attack is $\alpha = 32{\cdot}7^\circ$ and dimensionless time is $t^* = tU_\infty/C = 2{\cdot}55$. Minimum and incremental values of instantaneous vertical velocity contours in image are $v_{\min} = \pm 5$ (mm/s) and $\Delta v = 2{\cdot}5$ (mm/s), respectively. Dimensions of v are mm/s and z is mm.

7. CONCLUDING REMARKS

Techniques of high-image-density particle image velocimetry have led to the instantaneous and averaged patterns of velocity and vorticity associated with vortex breakdown, and its interaction with a stationary impingement plate. Vortex generation from both a stationary and a pitching delta wing has been considered. Images of the flow have been acquired in two principal planes: a plane coincident with the axis of the leading-edge vortex; and a plane parallel to the leading-edge of the impingement plate. Representations of the flow in these planes provide insight into the streamwise evolution of the vortex, including the occurrence of vortex breakdown and its interaction with the plate.

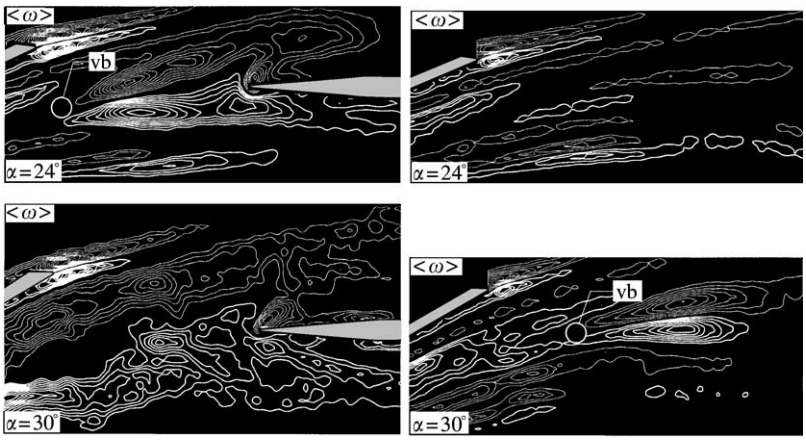

Figure 3(b). Contours of averaged vorticity $\langle\omega\rangle$ in the presence of the impingement plate (left column) and in the absence of the impingement plate (right column). In the presence of the impingement plate, minimum and incremental values of averaged vorticity $\langle\omega\rangle$ are $\omega_{\min} = \pm 1\ s^{-1}$ and $\Delta\omega = 0{\cdot}5\ s^{-1}$, respectively. In the absence of the impingement plate, minimum and incremental values of averaged vorticity $\langle\omega\rangle$ are $\langle\omega_{\min}\rangle = \pm 1\ s^{-1}$ and $\langle\Delta\omega\rangle = 0{\cdot}75\ s^{-1}$.

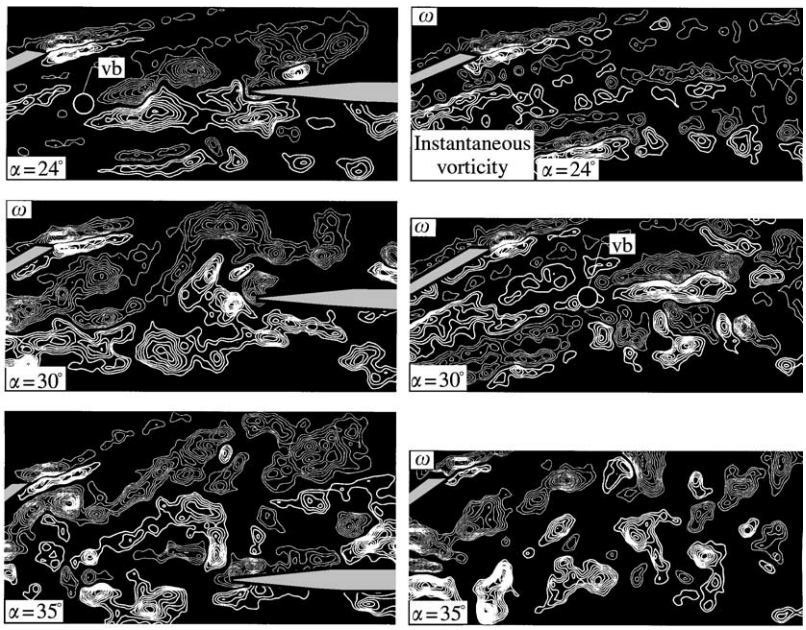

Figure 3(c). Contours of instantaneous vorticity ω in the presence of the impingement plate (left column) and in the absence of the impingement plate (right column). Minimum and incremental values of instantaneous vorticity ω are $\omega_{min} = \pm 1{\cdot}5\ s^{-1}$ and $\Delta\omega = 0{\cdot}75\ s^{-1}$, respectively, for all angles-of-attack in the presence of the impingement plate. In the absence of the impingement plate, minimum and incremental values of instantaneous vorticity ω for $\alpha = 24^\circ$ and 30° are, respectively, $\omega_{min} = \pm 1\ s^{-1}$ and $\Delta\omega = 0{\cdot}75\ s^{-1}$, and for $\alpha = 35^\circ$ are $\omega_{min} = \pm 2\ s^{-1}$ and $\Delta\omega = 0{\cdot}75\ s^{-1}$.

The case of the stationary delta wing and a stationary plate has served as a reference for characterization of the vortex–plate interaction. The locations of vortex breakdown, both in the presence of the impingement plate and in the absence of the plate, have been determined for incremental changes in angle-of-attack of the wing. It is demonstrated that, over a substantial range of angle-of-attack, the streamwise location of vortex breakdown is substantially different for the case with and without the impingement plate. This observation is conceptually similar to previous experiments, which have demonstrated an upstream movement of the onset of vortex breakdown due to the placement of a probe, moderate-sized cylinder, or a very small wire within or across the vortex. Taken together with the present results, it is clear that disturbances originating at the location of the leading-edge of the plate propagate upstream through the noncolumnar vortex to alter the steady-state location of vortex breakdown. This view is supported by the theoretical findings described in Section 3.

When the wing is subjected to pitching motion, the induced phase shift between the wing motion and the onset of vortex breakdown induces hysteresis loops of vortex breakdown position versus angle-of-attack. Remarkably, these loops are generally similar for cases with and without the impingement plate. In other words, despite the fact that wing motion induces a change in the vertical offset of vortex breakdown with respect to the leading-edge of the plate, the time variation of the axial location of breakdown along the vortex core is similar to the variation in absence of a plate. The consequence is the generation of essentially equivalent hysteretic-loops of breakdown position versus angle-of-attack. This equivalence of cases with and without the impingement plate is apparently due to the fact that the location of vortex breakdown never comes to an equilibrium state during its encounter with the leading-edge of the plate, due to the continuous variations of the vertical offset of the vortex center-line.

When the wing undergoes pitching motion, the vertical position of the incident vortex(ices) upon the plate, and thereby the mechanism of vortex–plate interaction, varies substantially during the pitching cycle. The incident vortex system is partitioned into two subsystems above and below the plate over a substantial range of angle-of-attack. The two vortices above the plate tend to merge together, while those below the plate move apart. In addition, a given vortex adjacent to the plate can induce either a distributed vorticity layer, or a vorticity concentration, depending upon the scale and circulation of the primary vortex.

These features of the partitioned vorticity field are also interpreted in terms of space–time distributions of vertical (transverse) velocity above and below the plate. According to the model of Breitsamter & Laschke (1994*a*, *b*, 1998), which is described in Section 1.3, these velocity distributions adjacent to the top and bottom surfaces of the plate can eventually be considered to determine the buffet-induced loading, provided the corresponding streamwise velocities are accounted for, and the effects of flow separation are not significant. The focus of the present investigation is on determination of the basic classes of patterns and topologies of both averaged and instantaneous fields of velocity vectors, in relation to fundamental types of vorticity patterns. Furthermore, the magnitude and form of the instantaneous distributions of velocity are assessed as a function of distance from the surface of the plate. The magnitude of the vertical component of the buffet velocity distribution is found to be sensitive to the elevation from the top or bottom surface of the plate, but the overall form of the distributions is generally preserved. It is recommended that a zonally averaged distribution of velocity be considered in order to characterize the normal buffet velocity. This aspect could be accounted for in the next generation of this work, which could employ a cinema version of particle image velocimetry to determine the space–time variations of both the vertical and horizontal velocity fields as a basis for the implementation of a model for the buffet loading.

ACKNOWLEDGMENTS

The support of the Air Force Office of Scientific Research under Contract No. F49620-99-1-0011, monitored by Dr Steven Walker, is gratefully acknowledged. One of the authors, Professor Besir Sahin, would like to thank the Scientific and Technical Research Council of Turkey (TUBITAK) and NATO for their financial support.

REFERENCES

AKILLI, H., SAHIN, B. & ROCKWELL, D. 2001 Control of vortex breakdown by a transversely-oriented wire. *Physics of Fluids* **13,** 452–463.

ASHLEY, H., ROCK, S. M., DIGUMARTHI, R. V., CHANEY, K. & EGGERS Jr., A. J. 1994 Active control for fin buffet alleviation. WL-TR-93-3099, Wright Patterson AFB, OH, January.

ATTA, R. & ROCKWELL, D. 1987 Hysteresis of vortex development and breakdown on an oscillating delta wing. *AIAA Journal* **25,** 1512–1513.

ATTA, R. & ROCKWELL, D. 1990 Leading-edge vortices on a pitching delta wing. *AIAA Journal* **28,** 995–1004.

BEAN, E. G. & WOOD, N. J. 1993 An experimental investigation of twin fin buffeting and suppression. AIAA Paper No. 93-0054.

BEUTNER, T. J., BAUST, H. N. & MEYERS, J. F. 1995 Doppler global velocimetry measurements of a vortex–tail interaction. *Proceedings of the 7th International Symposium on Flow Visualization*, Seattle, WA, U.S.A. (ed. J. P. Crowder), pp. 418–423. New York: Begell House.

BREITSAMTER, C. & LASCHKA, B. 1994*a* Turbulent flow structure associated with vortex-induced fin buffeting. *Journal of Aircraft* **31,**773–781

BREITSAMTER, C. & LASCHKA, B. 1994*b* Turbulent flowfield structure associated with fin buffeting around a vortex-dominated aircraft configuration at sideslip. 19*th Congress of the International Council of the Aeronautical Sciences*, Anaheim, CA, U.S.A. ICAS-94-4.3.2, Vol. I, 768–684.

BREITSAMTER, C. & LASCHKA, B. 1998 Fin buffet pressure evaluation based on measured flowfield velocities. *Journal of Aircraft* **35,** 806–815.

BROWN, G. L. & LOPEZ, J. M. 1990 Axisymmetric vortex breakdown. Part 2: physical mechanisms. *Journal of Fluid Mechanics* **221,** 553–576.

CANBAZOGLU, S., LIN, J.-C., WOLFE, S. & ROCKWELL, D. 1995*a* Buffeting of a fin: distortion of the incident vortex. *AIAA Journal* **33,** 2144–2150.

CANBAZOGLU, S., LIN, J.-C., WOLFE, S. & ROCKWELL, D. 1995*b* Buffeting of a fin: streamwise evolution of flow structure. *AIAA Journal of Aircraft* **33,** 85–190.

CIPOLLA, K. M. & ROCKWELL, D. 1998 Small-scale vortical structures in crossflow plane of a rolling delta wing. *AIAA Journal* **36,** 2276–2278.

DENG, Q. & GURSUL, I. 1997 Vortex breakdown over a delta wing with oscillating leading edge flaps. *Experiments in Fluids* **23,** 347–352.

DOLIGALSKI, T. L., SMITH, C. R. & WALKER, J. D. A. 1994 Vortex interactions with walls. *Annual Review of Fluid Mechanics* **26,** 573–616.

FERMAN, N. A., PATEL, S. R., ZIMMERMAN, N. H. & GERSTENKORN, G. 1990 A unified approach to buffet response of fighter aircraft empennage. *AGARD/NATO 70th Structures and Materials Meeting*, pp. 2-1-2-15. Sorento, Italy.

GEE, K., MURMAN, S. M. & SCHIFF, L. F. 1995 Computational analysis of F/A-18 tail buffet. AIAA Paper No. 95-3440.

GREENWELL, D. I. & WOOD, N. J. 1994 Some observations on the dynamic response to wing motion of the vortex burst phenomenon. *Aeronautical Journal* 49–59.

GORDNIER, R. E. & VISBAL, M. R. 1995 Instabilities in the shear layer of delta wings. AIAA Paper 95-2281, June.

GORDNIER, R. E. & VISBAL, M. R. 1997 Numerical simulation of the impingement of a streamwise vortex on a plate. AIAA Paper No. 97-1781. Also see 1999 *International Journal of Computational Fluid Dynamics* **12,** 49–66.

GURSUL, I. 2000 A proposed mechanism for the time lag of vortex breakdown location in unsteady flows. AIAA Paper No. 2000-0787.

GURSUL, I. & YANG, H. 1994 Vortex breakdown over a pitching delta wing. AIAA Paper 94-0536, 32nd Aerospace Sciences Meeting and Exhibit, January, Reno, NV.

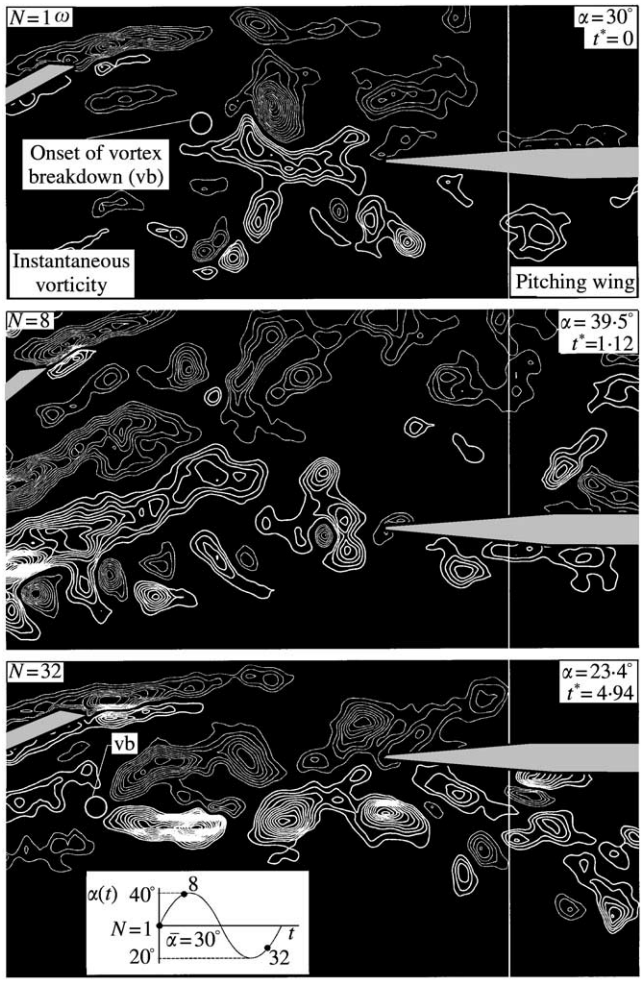

(a)

Figure 5(a). Patterns of positive (thick line) and negative (thin line) vorticity for pitching motion of delta wing in the presence of the impingement plate. Minimum and incremental values of instantaneous vorticity are $\omega_{min} = \pm 1.5\ s^{-1}$ and $\Delta\omega = 0{\cdot}75\ s^{-1}$, respectively. Mean angle-of-attack of delta wing $\bar{\alpha} = 30^\circ$ and amplitude of pitching motion is $\alpha_o = 10^\circ$. The reduced frequency is $k = \pi f_e C/U_\infty = 0{\cdot}74$ and dimensionless time $t^* = tU_\infty/C$.

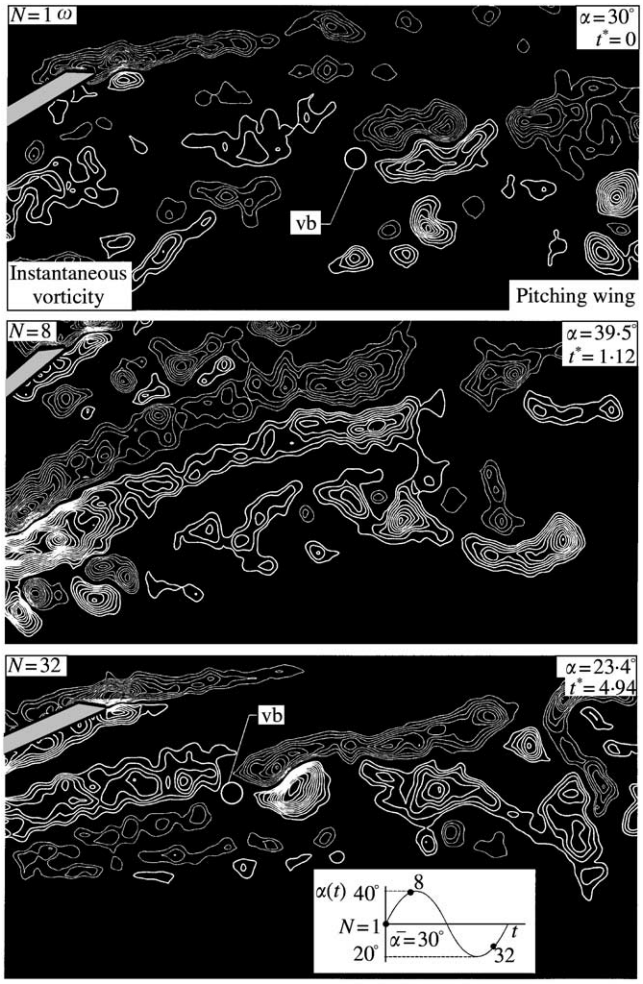

(b)

Figure 5(b). Patterns of positive (thick line) and negative (thin line) vorticity for pitching motion of delta wing in the absence of the impingement plate. Minimum and incremental values of instantaneous vorticity are $\omega_{min} = \pm 1{\cdot}5\ s^{-1}$ and $\Delta\omega = 0{\cdot}75\ s^{-1}$, respectively. Mean angle-of-attack of delta wing $\bar{\alpha} = 30^\circ$ and amplitude of pitching motion is $\alpha_o = 10^\circ$. The reduced frequency is $k = \pi f_e C/U_\infty = 0{\cdot}74$ and dimensionless time $t^* = tU_\infty/C$.

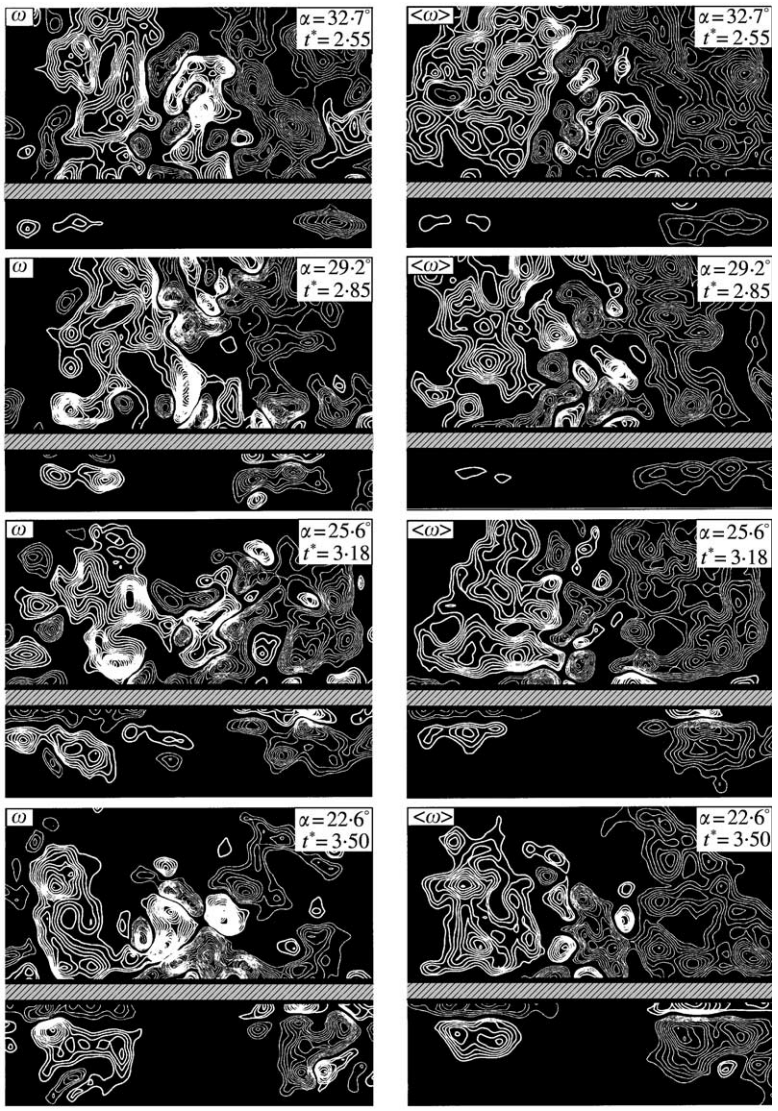

Figure 6(a). Cross-section of vortex breakdown–plate interaction at a location $0.185L_p$ downstream of the leading-edge of the plate, corresponding to the thin vertical line in Figure 5a. Delta wing is pitching at reduced frequency $k = \pi f_e C/U_\infty = 0{\cdot}74$. Instantaneous vorticity contours (left column) and averaged vorticity contours (right column) are represented as a function of angle-of-attack α of the wing and dimensionless time $t^* = tU_\infty/C$. Patterns of positive (thick line) and negative (thin line) vorticity are depicted. Minimum and incremental values of instantaneous vorticity are, respectively, $\omega_{\min} = \pm 1\ \mathrm{s}^{-1}$ and $\Delta\omega = 0{\cdot}5\ \mathrm{s}^{-1}$; and of averaged vorticity $\langle\omega\rangle$ are $\langle\omega_{\min}\rangle \pm 0.5\ \mathrm{s}^{-1}$ and $\langle\Delta\omega\rangle = 0{\cdot}35\ \mathrm{s}^{-1}$. Mean angle-of-attack and pitching motion amplitude of delta wing are $\bar{\alpha} = 30^\circ$ and $\alpha_o = 10^\circ$.

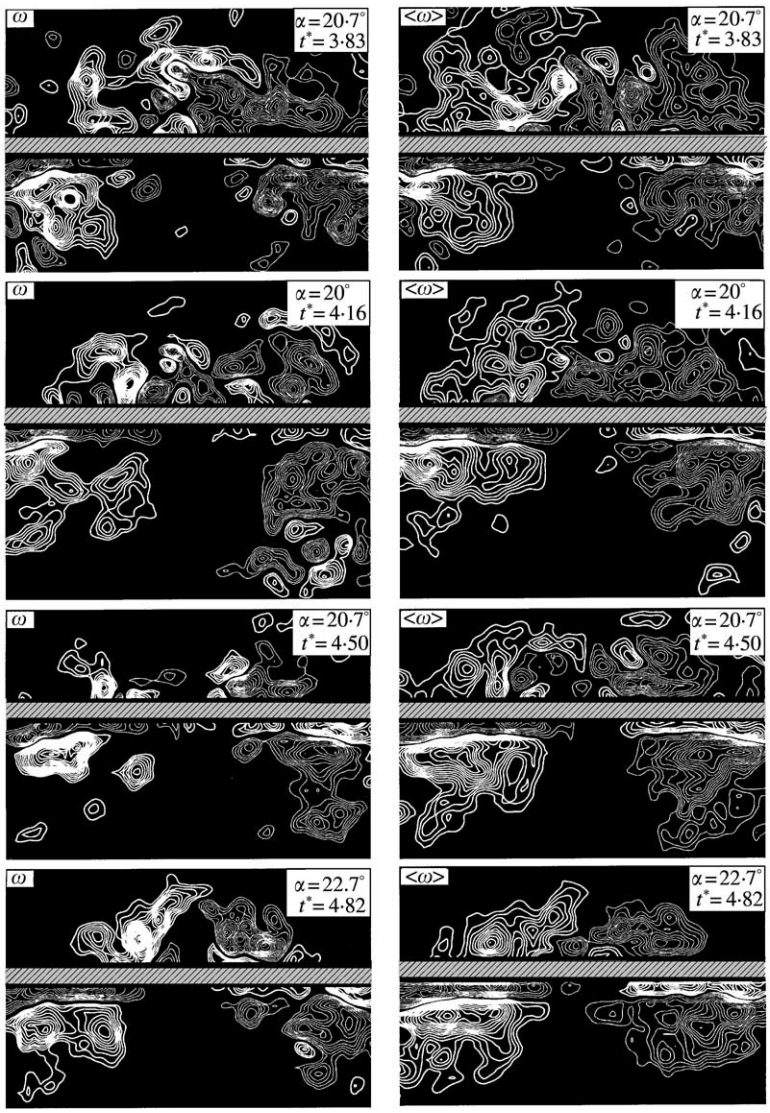

Figure 6(b). Cross-section of vortex breakdown–plate interaction at a location $0.185L_p$ downstream of the leading-edge of the plate, corresponding to the thin vertical line in Figure 5a. Delta wing is pitching at reduced frequency $k = \pi f_e C/U_\infty = 0{\cdot}74$. Instantaneous vorticity contours (left column) and averaged vorticity contours (right column) are represented as a function of angle-of-attack α of the wing and dimensionless time $t^* = tU_\infty/C$. Patterns of positive (thick line) and negative (thin line) vorticity are depicted. Minimum and incremental values of instantaneous vorticity are, respectively, $\omega_{\min} = \pm 1\ \mathrm{s}^{-1}$ and $\Delta\omega = 0{\cdot}5\ \mathrm{s}^{-1}$; and of averaged vorticity $\langle\omega\rangle$ are $\langle\omega_{\min}\rangle \pm 0.5\ \mathrm{s}^{-1}$ and $\langle\Delta\omega\rangle = 0{\cdot}35\ \mathrm{s}^{-1}$. Mean angle-of-attack and pitching motion amplitude of delta wing are $\bar{\alpha} = 30^\circ$ and $\alpha_o = 10^\circ$.

GURSUL, I. & YANG, H. 1995 On fluctuations of vortex breakdown location. *Physics of Fluids* **7,** 229–231.

GURSUL, I. & XIE, W. 2000 Interaction of vortex breakdown with an oscillating fin. AIAA Paper 2000-0279.

HUTTSELL, L. J., TINAPPLE, J. A. & WEYER, R. M. 1997 Investigation of buffet loading on a scaled f-15 twin tail model. AGARD Structures and Materials Panel Workshop, October, Denmark.

KANDIL, O. A., SHETA, E. F. & MASSEY, S. J. 1995 Buffet responses of a vertical tail in vortex breakdown flows. AIAA Paper No. 95-3464.

KANDIL, O. A. & SHETA, E. F. 1998 Coupled and uncoupled bending-torsion responses of twin-tail buffet. *Journal of Fluids and Structures* **12,** 677–701.

KUESSNER, H. G. 1954 A general method for solving problems of the unsteady lifting surface theory in a subsonic range. *Journal of the Aeronautical Sciences* **21,** 17–26.

LEE, B. H. K. 2000 Vertical tail buffeting of fighter aircraft. *Progress in Aerospace Sciences* **36,** 193–279.

LEE, B. H. K. & TANG, F. C. 1992 Buffet load measurements on an F/A-18 vertical fin at high angle-of-attack. AIAA Paper 92-2127.

LEE, B. H. K., BROWN, D., TANG, F. C. & PLOSENSKI, M. 1993 Flow field in the vicinity of an F/A-18 vertical fin at high angle-of-attack. *Journal of Aircraft* **30,** 69–74.

LEIBOVICH, S. 1984 Vortex stability and breakdown: survey and extension. *AIAA Journal* **22,** 1192–1206.

LEMAY, S. P., BATILL, S. M. & NELSON, R. C. 1990 Leading-edge vortex dynamics on pitching delta wing. *Journal of Aircraft* **27,** 131–138.

LOWSON, M. V. 1964 Some experiments with vortex breakdown. *Journal of the Royal Aeronautical Society* **68,** 343–xxx.

LUBER, W., BECKER, J. & SENSBURG, O. 1996 The impact of dynamic loads on the design of military aircraft. AGARD-R-815, Florence, Italy, pp. 8-1-8-27.

MAGNESS, C., ROBINSON, O. & ROCKWELL, D. 1993 Instantaneous topology of the unsteady leading-edge vortex at high angle-of-attack. *AIAA Journal* **31,** 1384–1391.

MARTIN, C. A. & THOMPSON, D. H. 1991 Scale model measurements on fin buffet due to vortex bursting on F/A-18″, AGARD/CP497.

MAYORI, A. & ROCKWELL, D. 1994 Interaction of a streamwise vortex with a thin plate: a source of turbulent buffeting. *AIAA Journal* **32,** 2022–2029.

MIAU, J. J., CHANG, R. C., CHOU, J. H. & LIN, C. K. 1992 Nonuniform motion of leading-edge vortex breakdown on ramp pitching delta wings. *AIAA Journal* **30,** 1691–1702.

MOSES, R. W. & HUTTSELL, L. 2000 Fin buffeting features of an early F-22 model. AIAA Paper No. 2000-1695.

MYOSE, R. Y., LEE, B. K., HAYASHIBARA, S. & MILLER, L. S. 1997 Diamond, cropped, delta and ouble-delta wing vortex breakdown during dynamic pitching. *AIAA Journal* **35,** 567–569.

ÖZGÖREN, M., SAHIN, B. & ROCKWELL, D. 2001 Perturbations of a delta wing: control of vortex breakdown and buffeting. *AIAA Journal of Aircraft*, in press.

REYNOLDS, G. A. & ABTAHI, A. A. 1987 Instabilities in leading-edge vortex development. AIAA Paper 87-2424.

RIZK, Y. M. & GEE, K. 1992 Unsteady simulation of viscous flow field around f-18 aircraft at large incidence. *Journal of Aircraft* **29,** 986–992.

RIZZETTA, D. P. 1996 Numerical simulation of the interaction between a leading-edge vortex in a vertical tail. AIAA Paper No. 96-2012.

ROCKWELL, D. 1993 Three-dimensional flow structure on delta wings at high angle-of-attack: experimental concepts and issues. AIAA Paper No. 93-0550.

SAHIN, B., AKILLI, H., LIN, J.-C. & ROCKWELL, D. 2001 Vortex breakdown-edge interaction: consequence of edge oscillations. *AIAA Journal*, **39,** 865–876.

SHAH, G. H. 1991 Wind-tunnel investigation of aerodynamic and tail buffet characteristics of leading-edge extension modifications to the F/A-18. AIAA Paper 91–2889.

SHETA, E. F., HARRAND, V. J. & HUTTSELL, L. J. 2000 Active vortical flow control for alleviation of twin-tail buffet of generic fighter aircraft. AIAA Paper No. 2000-0906.

THOMPSON, S. A., BATILL, S. M. & NELSON, R. C. 1991 Separated flowfield on a slender wing undergoing transient pitching motions. *Journal of Aircraft* **28,** 480–495.

TRIPLETT, W. E. 1983 Pressure measurements on twin vertical tails in buffeting flow. *Journal of Aircraft* **20,** 920–925.

WANG, S. & RUSAK, Z. 1997 The dynamics of a swirling flow in a pipe and transition to axisymmetric vortex breakdown. *Journal of Fluid Mechanics* **340,** 177–223.

RUSAK, Z., WANG, S. & WHITING, C. H. 1998 The evolution of a perturbed vortex in a pipe to axisymmetric vortex breakdown. *Journal of Fluid Mechanics* **366,** 211–237.

WASHBURN, A. E., JENKINS, L. M. & FERMAN, M. A. 1993 Experimental investigation of vortex-fin interaction. AIAA Paper 93-0050.

WENTZ JR, W. H. 1987 Vortex-fin interaction on a fighter aircraft. AIAA Paper 87-4909.

WOFFELT, K. W. 1987 Investigation of the movement of vortex burst position with dynamically changing angle of attack for a schematic delta wing in water tunnel with correlation to similar studies in a wind tunnel. *Aerodynamic and Related Hydrodynamic Studies Using Water Facilities.* AGARD-CP-413.

WOLFE, S., LIN, J.-C. & ROCKWELL, D. 1995*a* Buffeting of fins: an assessment of surface pressure loading. *AIAA Journal* **33,** 2232–2235.

WOLFE, S., LIN, J.-C. & ROCKWELL, D. 1995*b* Buffeting at the leading-edge of a flat plate due to a streamwise vortex: flow structure and surface pressure loading. *Journal of Fluids and Structures* **9,** 359–370.

YANG, H. & GURSUL, I. 1997 Vortex breakdown over unsteady delta wings and its control. *AIAA Journal* **35,** 571–574.

ZIMMERMAN, N. H., FERMAN, M. A., YURKOVICH, R. N. & GERSTENKORN 1989 Prediction of tail buffet loads for design application. AIAA Paper No. 89-1378.